

Figure 1. Common sex determination systems in insects. With male heterogamety, males have heteromorphic sex chromosomes (XY), and females are homomorphic (XX). With female heterogamety, females have heteromorphic sex chromosomes (ZW), and males are homomorphic (ZZ). Under haplodiploid sex determination, females develop from diploid fertilized eggs (nn), and males develop from unfertilized haploid eggs (n). Under PGE, males develop from initially fertilized eggs, but eliminate their paternal genome during development (and become functionally haploid). Sperm are shown in blue, and eggs are shown in red. M indicates meiosis, F indicates fertilization, and PGE the elimination of the paternal genome.

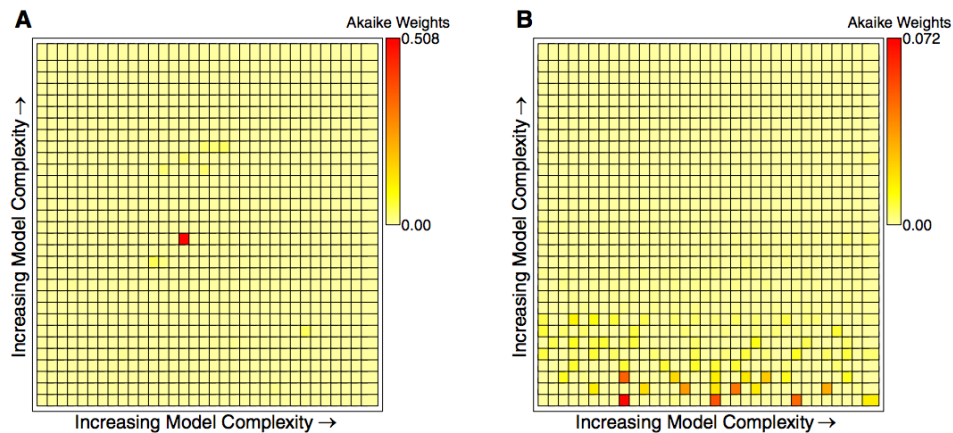


Figure 5. Visual depictions of model space for the genetic architecture of reproductive isolation in *T. castaneum*. Each box represents a genetic architecture model is colored to reflect its w_i . The scale ranges from lightest for models with w_i of zero to darkest for those with the maximum value for the analysis. Models are organized with the simplest model at the lower left and increase in complexity upward and to the left, that is, all one-parameter models are on the bottom row followed by two-parameter models when the right edge of the graph is reached a second row is added on top of the first. (A) Results from the analysis of dataset 4 showing low model selection uncertainty. (B) Results from the analysis of dataset 6 showing considerable model selection uncertainty.

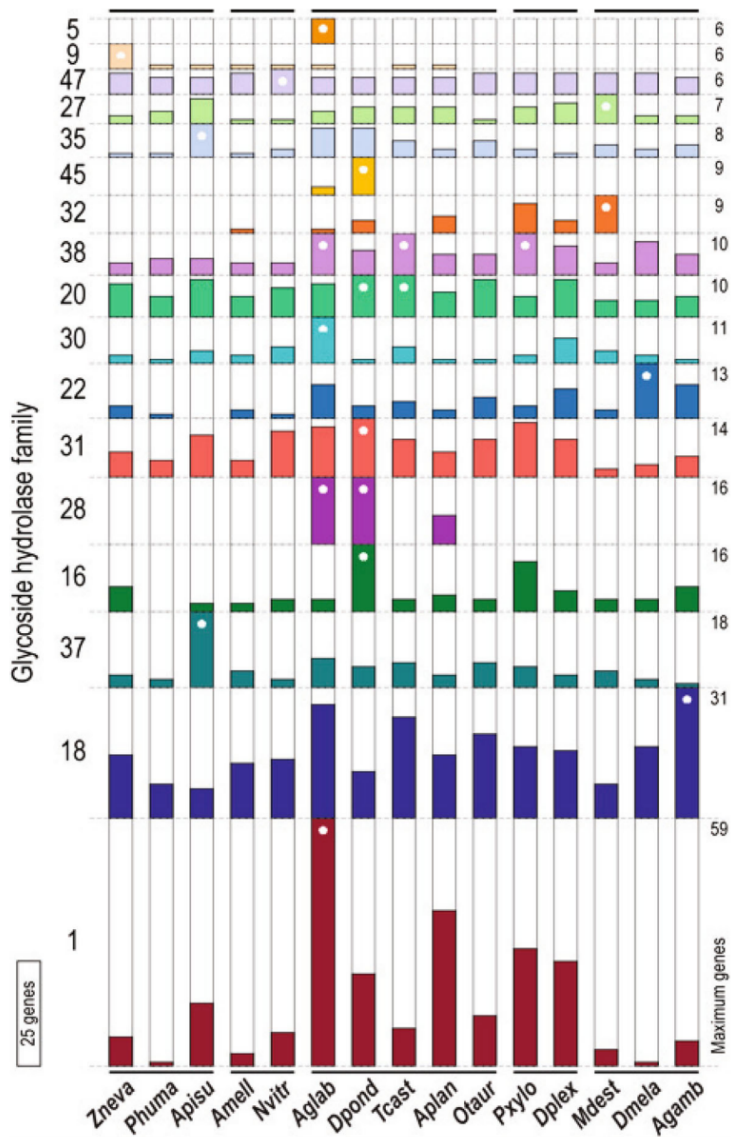


Fig. 4 Sub-family sizes for glycoside hydrolases found in the genome sequences of 15 insect species, including *A. glabripennis*. Species with the maximum gene count for each are indicated with a white asterisk. Among the examined species, *A. glabripennis* showed the most genes with matches to GH domains, the majority of which were found as multi-copy orthologs. This elevated gene count was mainly due to GH family 1 (IPR001360), members of which exhibit beta-glucosidase, beta-galactosidase, 6-phospho-beta-galactosidase, 6-phospho-beta-glucosidase, lactase-phlorizin hydrolase, beta-mannosidase, and myrosinase activities. Uniquely among the examined species, six *A. glabripennis* genes matched GH family 5 (IPR001547), also known as cellulase family A, whose members exhibit endoglucanase, beta-mannanase, exo-1,3-glucanase, endo-1,6-glucanase, xylanase, and endoglycoceramidase activities. *A. glabripennis* also had two matches to the GH family 45 (IPR000334, endoglucanase activity), also known as cellulase family K, which was also found in *D. ponderosae* (nine copies). Members of GH family 28 (IPR000743) are pectinases that exhibit polygalacturonase and rhamnogalacturonase activities and had matches to 16 genes in *A. glabripennis* (18 were identified by manual annotation; 19 were reported in [8]), 16 in *D. ponderosae* and 7 in *A. planipennis* (50 were manually annotated)

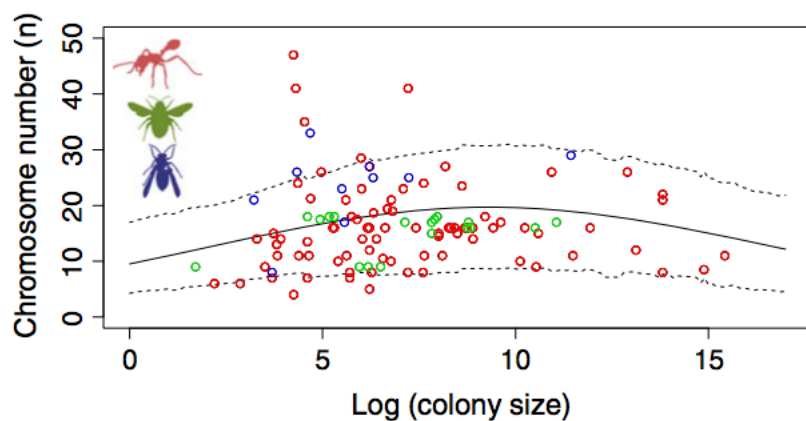
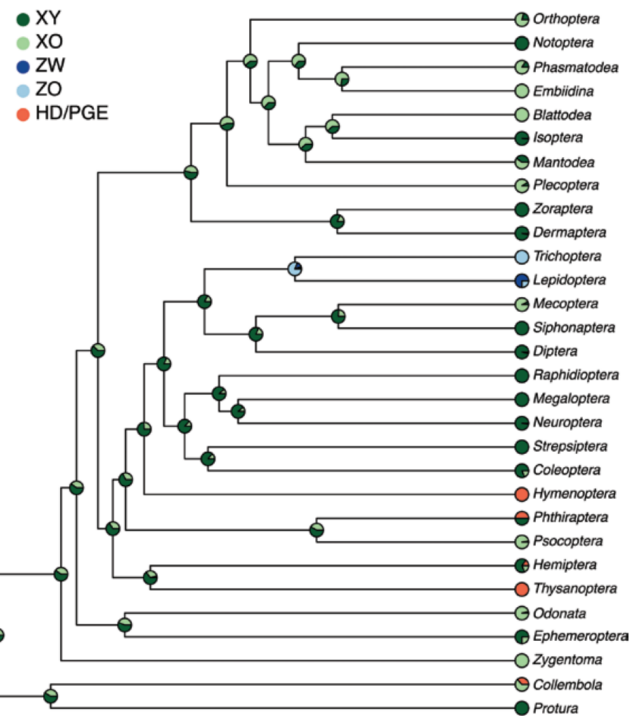


Fig. 3 The correlation between chromosome number and colony size. The open dots show the raw data, whereas the solid lines show the model estimation from a phylogenetic mixed model in MCMCglmm generated using the ‘predict’ function. The dotted lines show the 95% credibility interval around the estimates. Data from different taxonomic groups are colour-coded (ants = red, bees = green and wasp = blue).

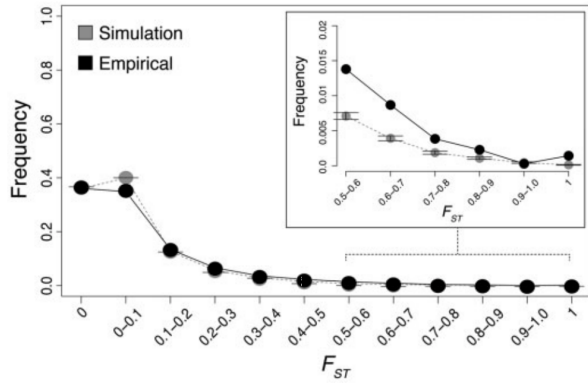
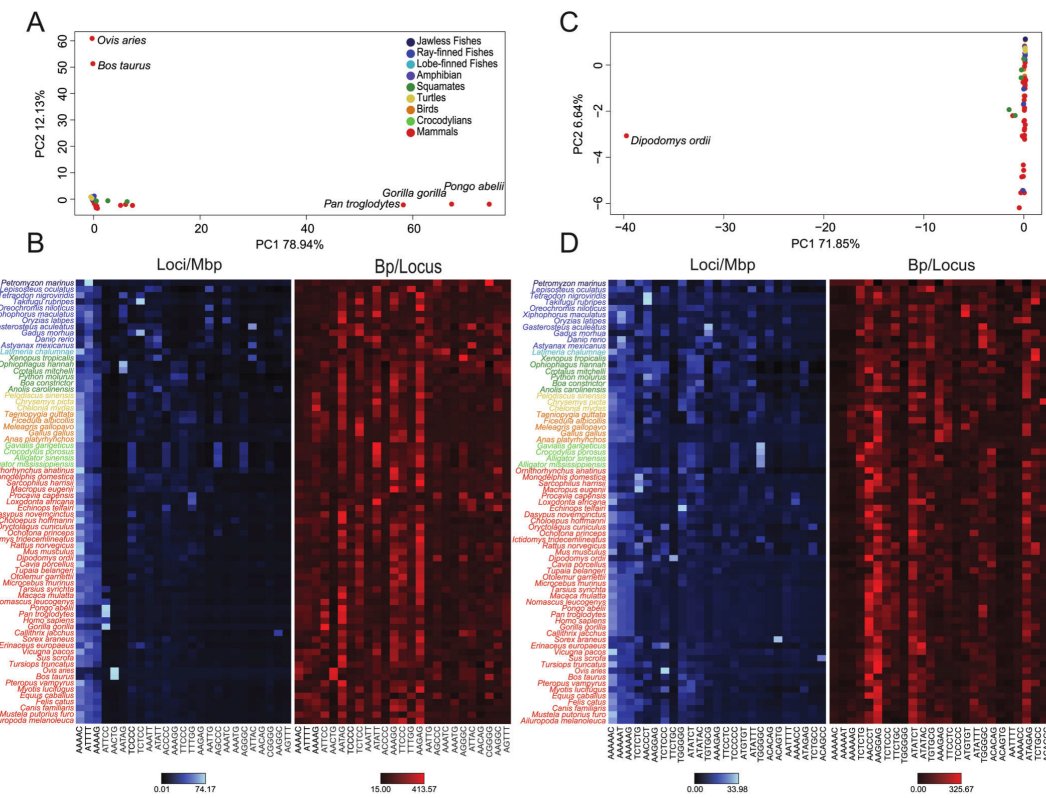


Fig. 1. Empirical and posterior predictive simulated (PPS) distributions of F_{ST} for example data, with standard deviations. The mean proportion of loci from the 100 replicate PPS runs (gray) and proportion of loci in the empirical data (black) are shown. Inset (top-right) shows upper limit of the F_{ST} distribution



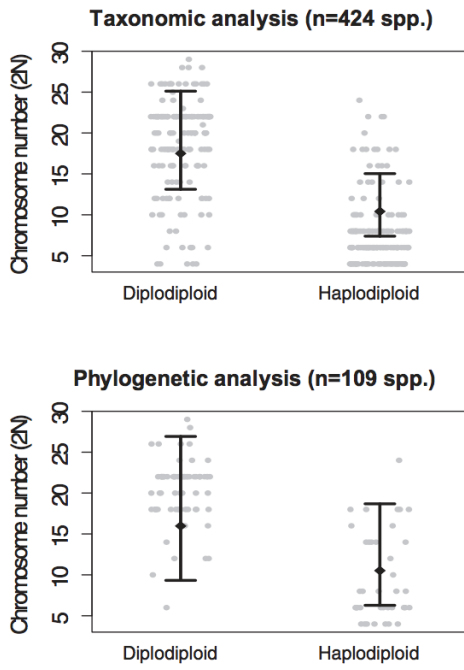


Figure 2. The relationship between chromosome number and ploidy across the Acari. (A) Scatterplot of all available estimates of chromosome number of haplodiploid and diploidiploid taxa for which taxonomic data were available. The black diamonds and error bars show the model prediction (posterior mean and 95% CI) of a taxonomic mixed model in MCMCglmm. (B) Scatterplot of all available estimates of chromosome number of haplodiploid and diploidiploid taxa for which phylogenetic data were available. The black diamonds and error bars show the model prediction (posterior mean and 95% CI) of a phylogenetic mixed model in MCMCglmm.

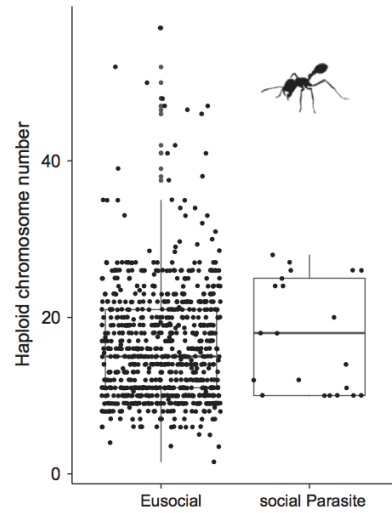


Fig. 5 Chromosome number comparison between social parasites and their eusocial relatives. Haploid chromosome numbers. We only consider those social parasites that completely lack their own worker caste. The boxplot shows the interquartile range that contains values between 25th and 75th percentile. The line inside the box shows the median. The two ‘whiskers’ show the largest/smallest observation that is less than or equal to the upper quartile plus/minus 1.5 the length of the interquartile range.

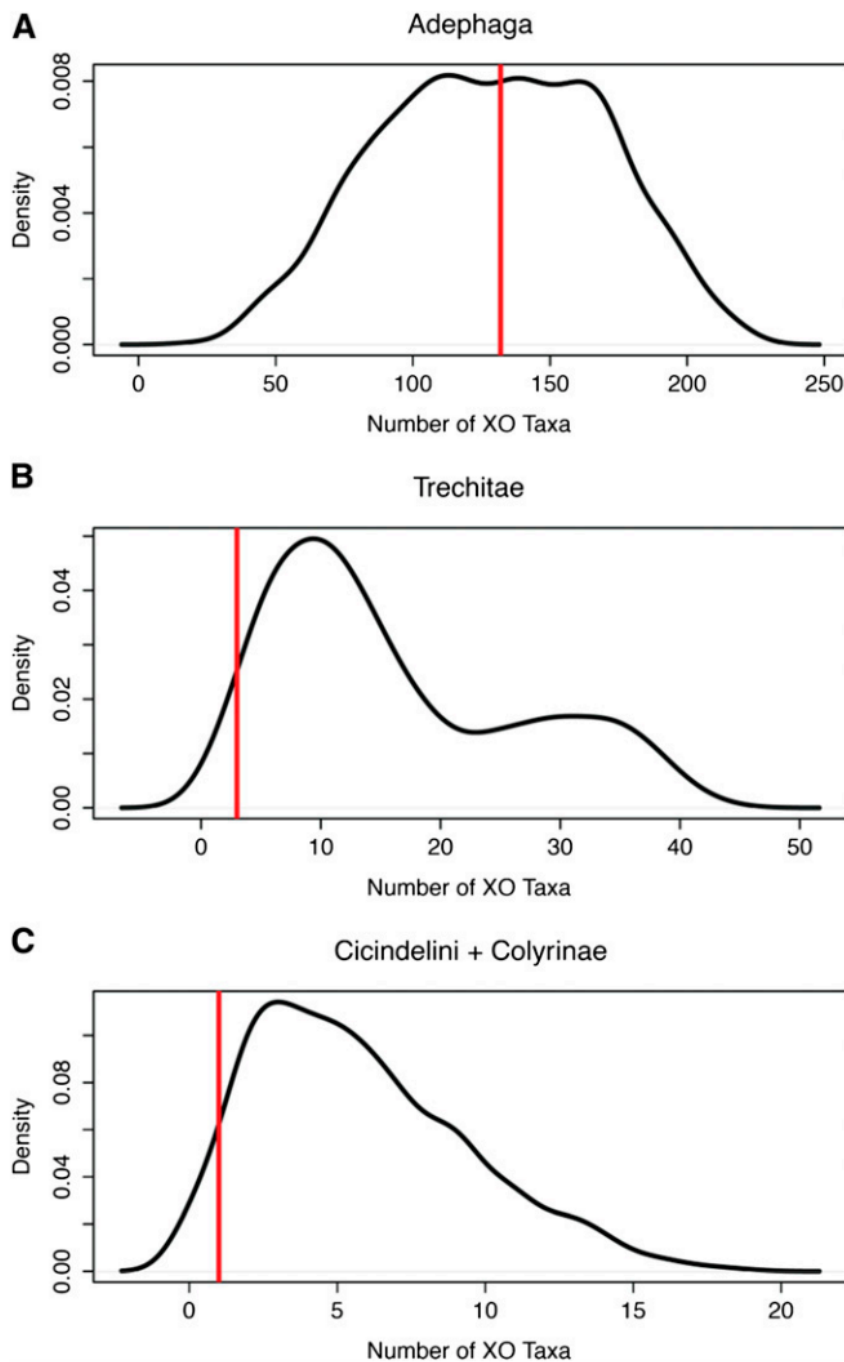


Figure 5 Distribution of PPS datasets in the suborder Adephaga. The black lines indicate the density of simulated datasets; the vertical red lines indicate the number of taxa observed in the XY state. (A) Adequate performance of model 2.1 in Adephaga is evident by the concentration of datasets similar to the observed data. The poor performance of model 2.1 in the subtrees composed of the clades Trechitae (B) and Cicindelini + Colyrinae (C) is evidence that these clades have higher retention rates of the Y chromosome than is expected for groups in the suborder Adephaga.

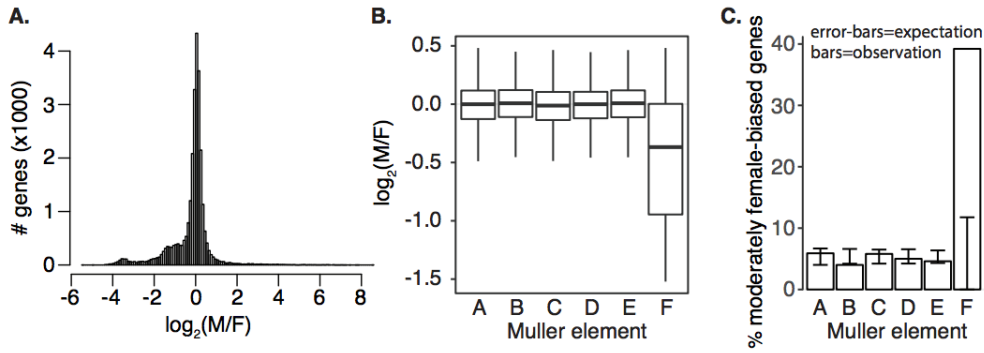


Figure 2: Muller element F is the cockroach X chromosome. The distributions of $\log_2 \frac{M}{F}$ for (A) annotated genes in the *B. germanica* genome and (B) genes with *D. melanogaster* homologs on each Muller element are shown. (C) The percent of *B. germanica* genes with moderately female-biased coverage ($\log_2 \frac{M}{F} < -0.5$) that have *D. melanogaster* homologs in each of the 6 Muller elements is plotted. The 95% confidence intervals (CIs) of the expected number of genes for each Muller element are shown by the error bars. Observed percentages that lie outside the CI indicate an excess or deficiency of genes on an element with moderately female-biased coverage.

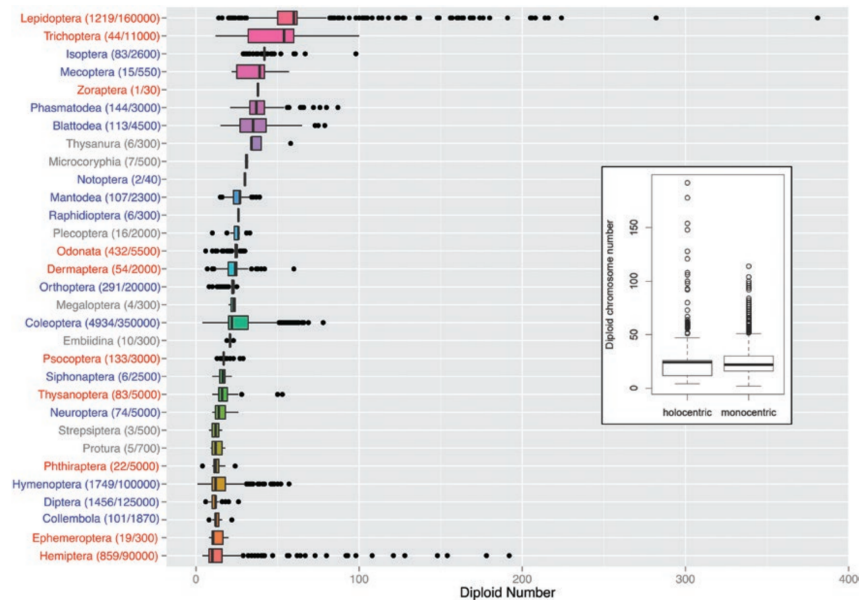
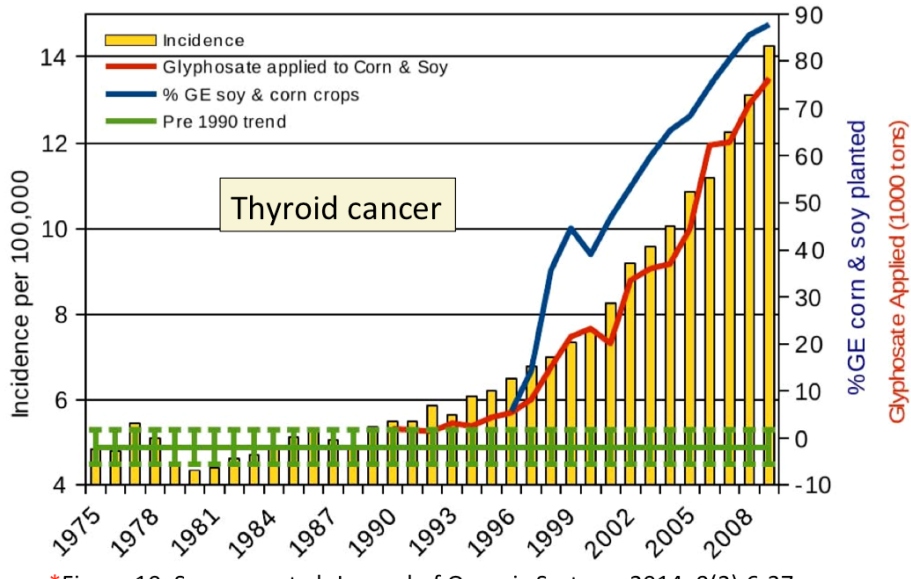


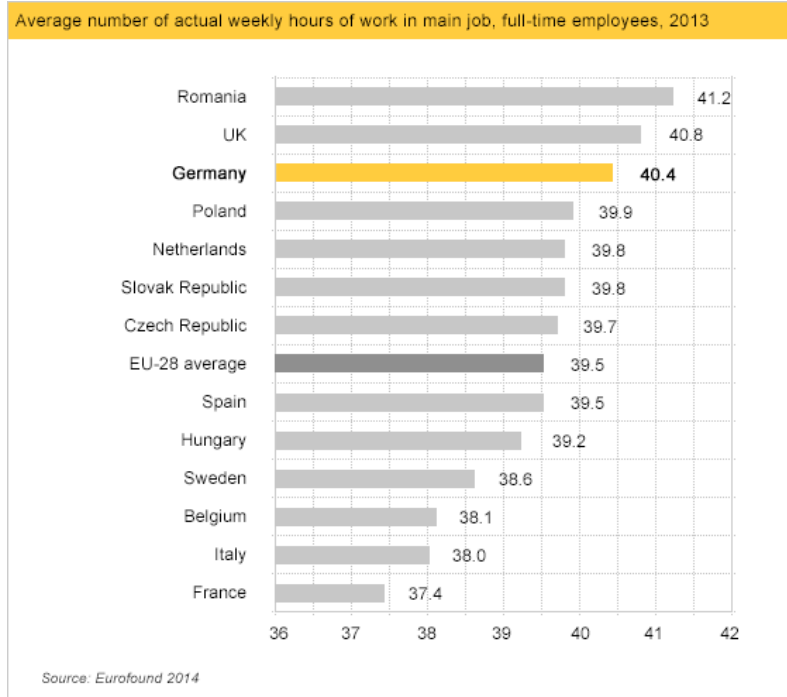
Figure 5. Distribution of chromosome numbers across hexapods. Diploid chromosome numbers are reported. Boxes represent the range of 25th to 75th percentile. Outliers are plotted as individual points. The color of the order names indicates whether chromosomes are holocentric (red), monocentric (blue), or unknown (gray). The number of species for which data is available and the size of each order is indicated in parentheses. The insert shows diploid chromosome numbers for holocentric versus monocentric species (Melters et al. 2012), where boxes represent the range of 25th to 75th percentile, and individual points the outliers.

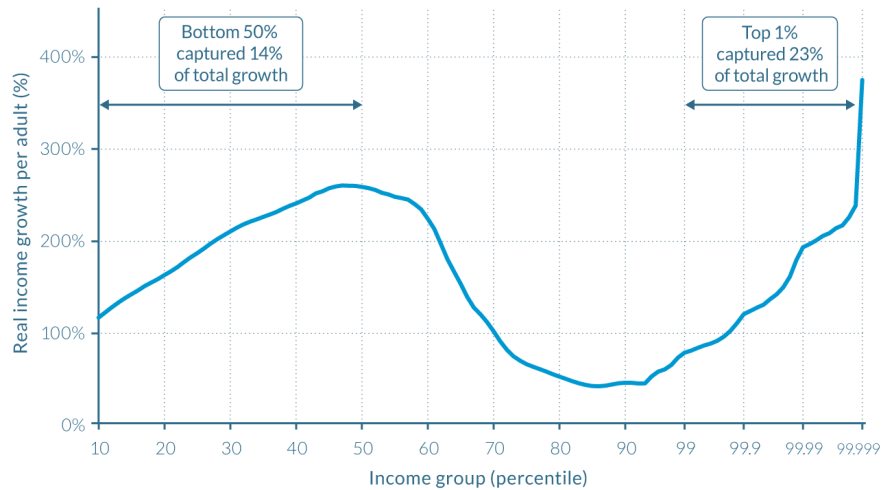
Thyroid Cancer Incidence Rate (age adjusted)

plotted against glyphosate applied to U.S. corn & soy ($R = 0.988$, $p \leq 7.612e-09$)
 along with %GE corn & soy crops $R = 0.9377$, $p \leq 2.152e-05$
 sources: USDA:NASS; SEER



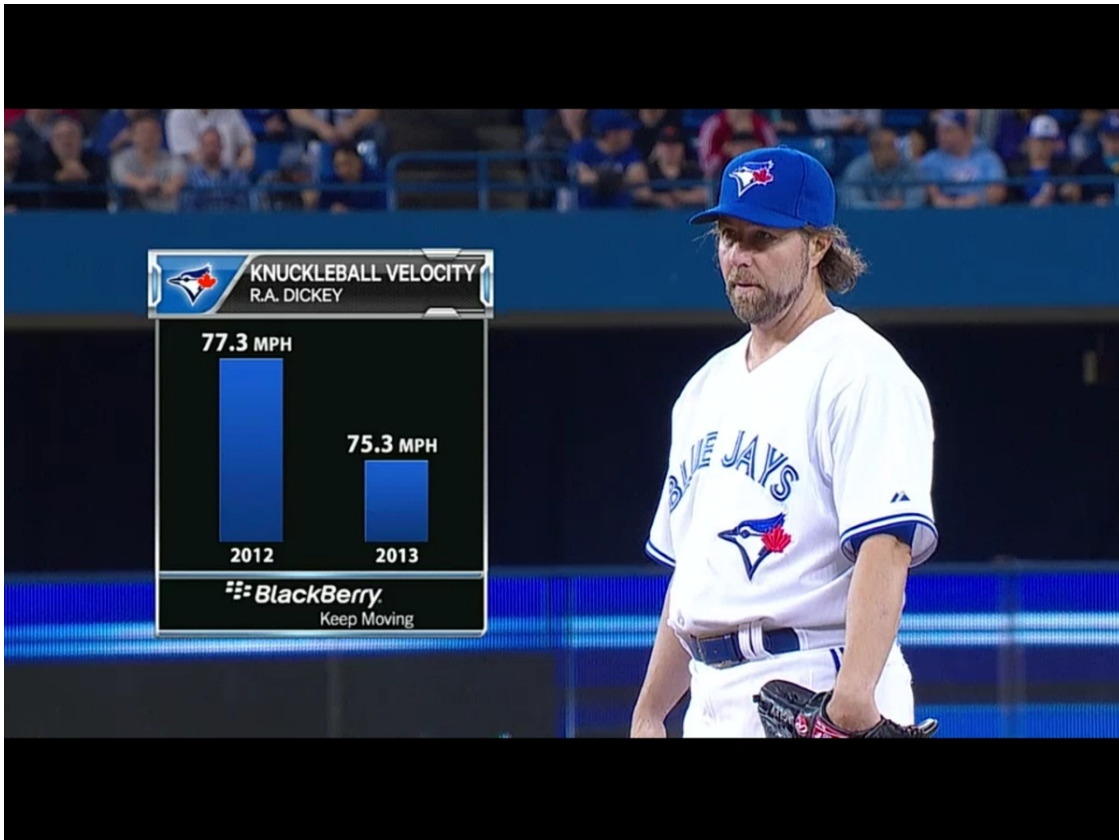
*Figure 10, Swanson et al. Journal of Organic Systems 2014; 9(2):6-37.

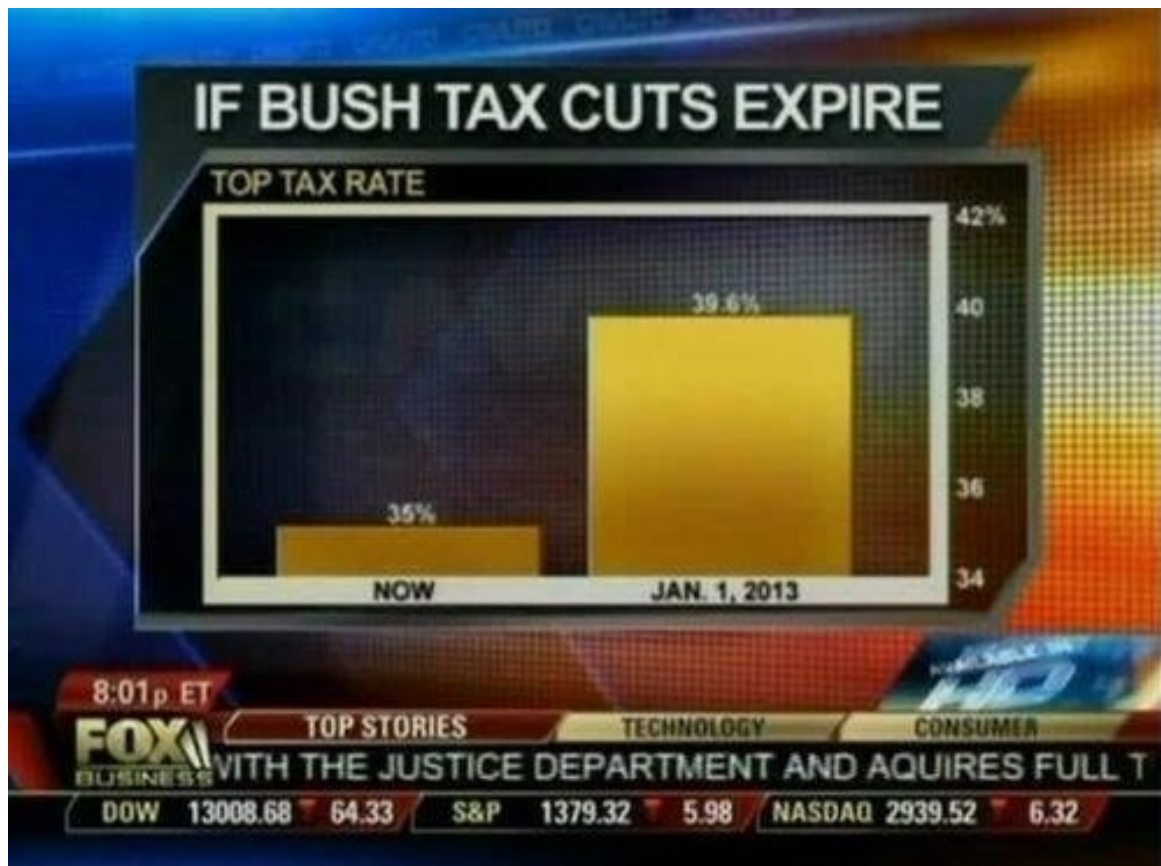




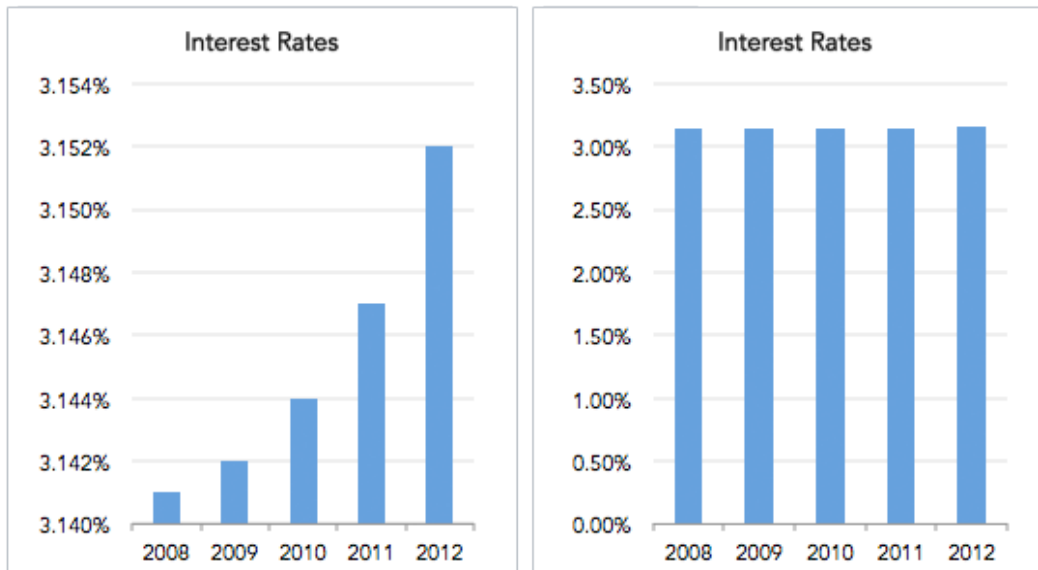
Source: WID.world (2017). See wid.world/methodology.html for data series and notes.

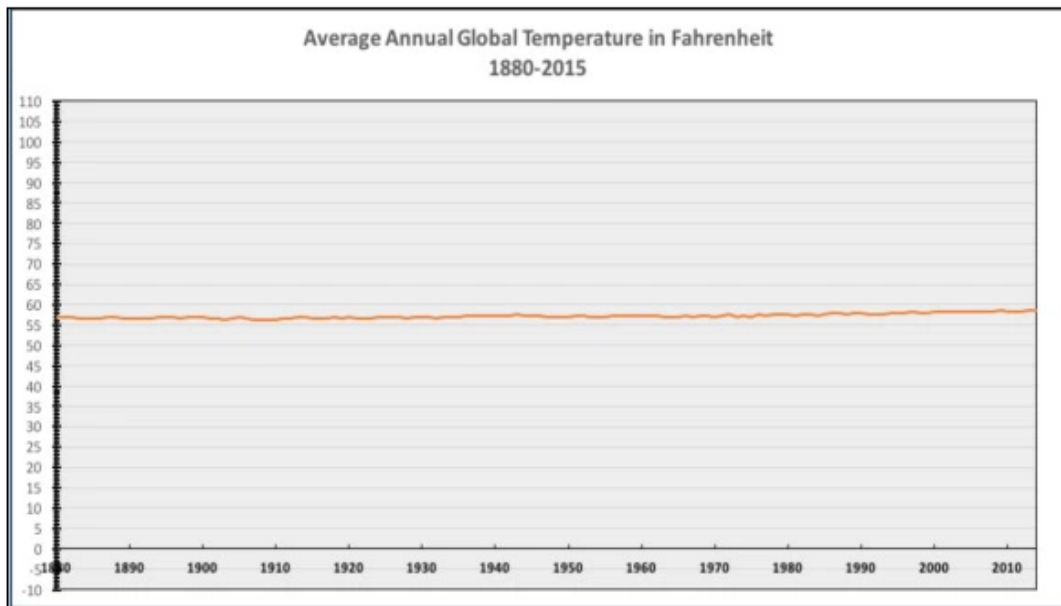
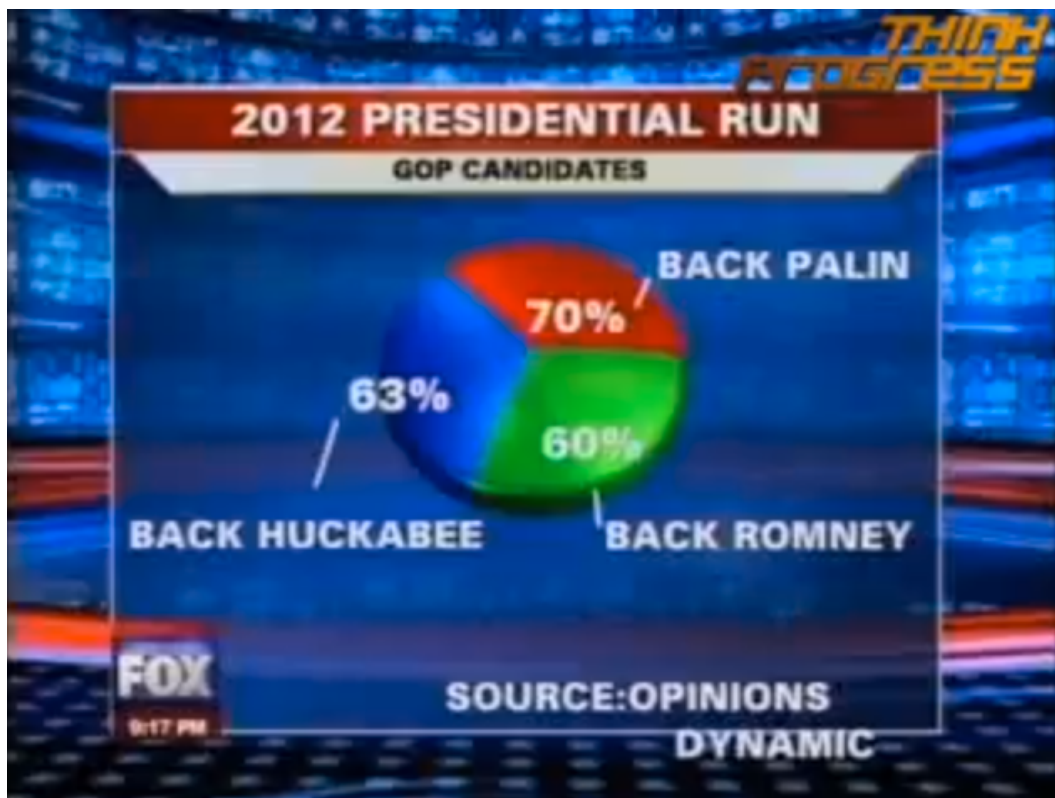
On the horizontal axis, the world population is divided into a hundred groups of equal population size and sorted in ascending order from left to right, according to each group's income level. The Top 1% group is divided into ten groups, the richest of these groups is also divided into ten groups, and the very top group is again divided into ten groups of equal population size. The vertical axis shows the total income growth of an average individual in each group between 1980 and 2016. For percentile group p99p99.1 (the poorest 10% among the world's richest 1%), growth was 77% between 1980 and 2016. The Top 1% captured 23% of total growth over this period. Income estimates account for differences in the cost of living between countries. Values are net of inflation.

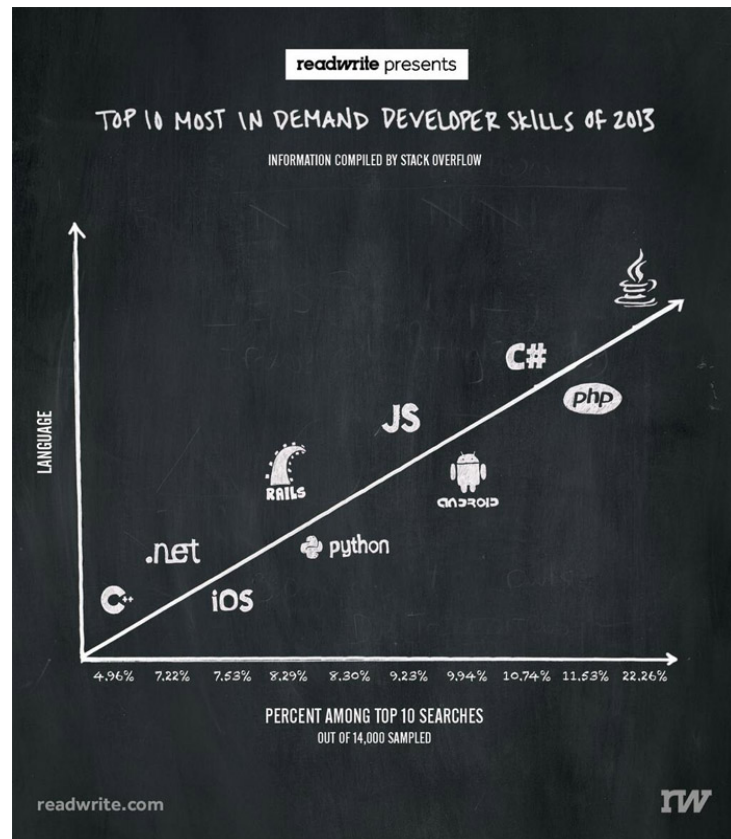




Same Data, Different Y-Axis

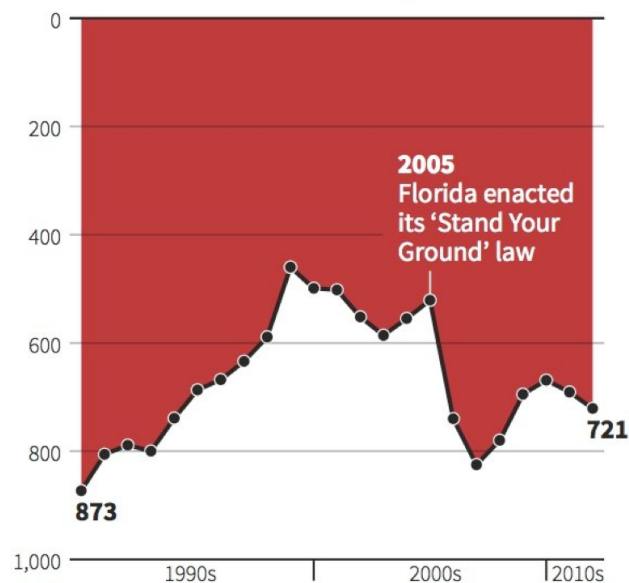






Gun deaths in Florida

Number of murders committed using firearms



Source: Florida Department of Law Enforcement

C. Chan 16/02/2014

REUTERS